The current issue and full text archive of this journal is available at
www.emeraldinsight.com/0961-5539.htm

Received 17 November 2008
Revised 10 June 2009
Accepted 29 July 2009

Effects of heat transfer on the strength of shock waves emitted upon spherical bubble collapse

Miralam Mahdi, Mehrzad Shams and Reza Ebrahimi
Faculty of Mechanical Engineering, K.N. Toosi University of Technology, Tehran, Iran

Abstract

Purpose – The purpose of this paper is to study numerically the effects of heat transfer on the strength of shock waves emitted upon spherical bubble collapse.

Design/methodology/approach – The motion of bubble under ultrasound is predicted by solutions of the Navier-Stokes equations for the gas inside a spherical bubble. The Gilmore model and the method of characteristics are used to model the shock wave emitted at the end of the bubble collapse.

Findings – The theory permits one to predict correctly the bubble radius-time curve and the characteristics of shock wave in sulphuric acid solution. These simulations indicated that the heat transfer inside the bubble and the liquid layer plays a major role in the bubble behaviour and the strength of the shock waves. Also, the developed numerical scheme is checked for different gas bubble like air, Argon and Xenon. It is observed that the gas thermal conductivity plays an important role in the shock wave strength. A good agreement is observed by comparison of the results with the experimental data.

Originality/value – The effect of heat transfer on the emitted shock wave strength has not been studied previously. In this paper, a numerical scheme is developed to consider heat transfer on the shock. Also, this simulation is checked for different gas conductivities.

Keywords Sulphuric acid, Waves, Heat transfer, Gas technology, Thermal conductivity
Paper type Research paper

Nomenclature

C speed of sound at the interface between the gas – filled bubble and the liquid, m/s

c speed of sound in the bulk liquid, m/s

C_v heat capacity at constant volume, J/kg K

C_p heat capacity at constant pressure, J/kg K

e internal energy per mass, J/kg

f frequency of driving pressure, Hz

h enthalpy in the bulk liquid, J/kg

H liquid enthalpy at the interface between the gas – filled bubble and the liquid, J/kg

k_g gas heat conductivity, W/mK

k_l liquid heat conductivity, 0.4 W/mK

m gas mass inside a bubble, kg

p pressure in the liquid, pa

P pressure at the bubble interface, pa

p_b pressure inside the bubble, pa

$P_{b\circ}$ pressure at bubble centre, pa

P_e driving pressure amplitude, pa

q heat transfer conducted through the gas, W

R bubble radius, m

r radial distance to the bubble centre, m

$R_\circ$ initial bubble radius, m

$\dot{R}$ bubble wall velocity, m/s

$\ddot{R}$ bubble wall acceleration, m/s^2

t time, s

T_b temperature inside the bubble, K

T_{bl} temperature at bubble-liquid interface, K

International Journal of Numerical Methods for Heat & Fluid Flow
Vol. 20 No. 4, 2010
pp. 372-391

0961-5539
DOI 10.1108/09615531011035794

$T_{b\circ}$ temperature at the bubble centre, K

T_∞ Liquid temperature far from the bubble, K

u(t) velocity in the liquid, m/s

u_g radial velocity profile inside the bubble, m/s

Greek symbols

γ specific heat ratio

σ surface tension of the liquid, 0.055 N/m

μ dynamic viscosity of the liquid, $0.025\,\mathrm{Ns/m^2}$

ρ liquid density, $\mathrm{kg/m^3}$

$\rho_\circ$ ambient liquid density, $1{,}800\,\mathrm{kg/m^3}$

Subscripts

b bubble

l liquid

bl bubble liquid interface

∞ ambient liquid medium

1. Introduction

In an acoustic field, matter is alternately subjected to pressure and tension. In the tension phase, a liquid rupture to form cavities or bubbles in the liquid that finally close when the tension is released for longer time. The pressure in liquid increases to a positive value in the pressure phase. As a consequence, the bubble decreases in size violently, overshooting its equilibrium size and bouncing back (whenever it does not break). This process is usually referred to as the collapse and rebound of the bubble. The velocity and pressure fields in the liquid are caused by the shock waves originating from the rapidly rebounding bubble wall.

The equations of motion governing these effects were started by Lord Rayleigh in the 19th century (Hilgenfeldt *et al.*, 1998). The formalism was substantially refined and developed by Plesset, Prosperetti, and others over a span of several decades. Usually, the Rayleigh-Plesset equation for the bubble wall motion and the polytropic relation for the gas behaviour inside the bubble under ultrasound have been employed. If the heat transfer is fast (relative to the time scale of the bubble motion), then the gas in the bubble is maintained at the temperature of the liquid, and the pressure is determined by an isothermal equation of state. On the other hand, if the bubble wall moves very quickly relative to the time scale of heat transfer, then heat will not be able to escape from the bubble, and the bubble will heat adiabatically on collapse. If the rate of heat transfer is intermediate between adiabatic and isothermal, the situation is more complicated. Hence, a correct calculation requires solving the heat conduction problem throughout the bubble cycle and using the computed temperature in the bubble to evaluate the pressure in the gas. This is quite a difficult task. Over the years, several methods have been proposed that amount to varying polytropic index continuously between the isothermal value and the adiabatic value (Plesset and Prosperetti, 1997; Prosperetti, 1977; Kamath *et al.*, 1993). This approach can yield quantitatively incorrect results in large part because energy dissipation from thermal processes is neglected (Prosperetti and Hao, 1999). Wu and Robert (1993) and Moss *et al.* (1994) tried to solve numerically the total energy equation without considering the heat transfer inside the bubble and the liquid layer at the bubble wall. However, their calculation overestimated the gas temperature in the bubble. Prosperetti (1977) solved the internal energy equation combined with the mass and momentum equation numerically to consider heat transport inside the bubble. However, heat transfer through the liquid layer was not considered in their study. While Kwak and Na (1996) considered the quadratic

temperature distribution in the liquid layer adjacent to the bubble wall and provided a time-dependent first-order equation thermal boundary layer thickness.

In many practical bubble-collapse situations, however, it appears that local velocities reach an appreciable fraction of the velocity of sound in the liquid, and the compressibility of the liquid cannot safely be neglected. Early work on collapse focused on the inclusion of liquid compressibility in order to learn more about the production of shock waves. Herring (1941) derived the first-order correction of the ratio of liquid velocity to sonic velocity. Later, Schneider (1949) treated the same, highly idealized problem by numerically solving the equations of compressible flow. Gilmore (1956) showed that one could use the approximation introduced by Kirkwood and Bethe (1942), which assume that in the final stage of collapse the inertial motion prevails upon the acoustic effect, to obtain analytic solutions.

From an experimental viewpoint, the dynamics of spherical, isolated bubbles driven by an acoustic wave have been measured using light scattering methods (Weninger *et al.*, 2001). However, the main direct experimental observations of bubble collapse near a solid surface have been obtained upon laser-induced cavitation (Philipp and Lauterborn, 1998). The strength of the cavitation shocks and their range of action have been studied in detail by Hickling and Plesset (1964). Hickling and Plesset were the first to make use of numerical solutions of the compressible flow equations to explore the formation of pressure waves or shocks during the rebound phase. Other numerical calculations have since been carried out by Ivany and Hammitt (1965), Tomita and Shima (1977), and Fujikawa and Akamatsu (1980), among others. Ivany and Hammitt confirmed that neither surface tension nor viscosity play a significant role in the problem. Recently, Minsier and Proost (2007) showed the importance of equation of state on the shock wave velocity emitted upon bubble collapse.

In this paper, shock wave emission resulting from spherical bubble collapse is modelled in sulphuric acid. A set of the Navier-Stokes equations for the gas inside a spherical bubble with considering heat transfer through the gas inside the bubble and the liquid layer is solved. It shows that the polytropic relation with conjunction the Gilmor equation provides considerable overestimation of the peak pressure and underestimation of the peak temperature for an ultrasonic gas bubble. The outward-travelling shock wave strength and velocity is compared with polytropic state and present model. The most of previous studies are not considered the heat transfer inside the gas bubble. This investigation shows that this effect is very important and should be considered.

2. Hydrodynamic bubble motion

Consider a spherical bubble of radius, $R(t)$ (where t is time), in an infinite domain of liquid (85 per cent sulphuric acid solution) whose temperature and pressure far from the bubble are T_∞ and $P_\infty(t)$, respectively. A sketch of the bubble model used is given in Figure 1. The temperature, T_∞, is assumed to be simple constant since temperature gradients were eliminated and uniform heating of the liquid due to internal heat sources or radiation will not be considered. On the other hand, the pressure, $P_\infty(t) = P_\circ + P_e \sin(2\pi ft)$, is assumed to be a known controlled input which regulates the growth or collapse of the bubble. P_e and f are the driving pressure amplitude and frequency respectively and $P_\circ = 1$ bar is ambient pressure. Mass transfer through the bubble interface and evaporation or condensation of liquid molecules near the interface was not considered in this analysis. Heat transfer was assumed to occur through the thermal boundary layer having thickness of $\delta(t)$.

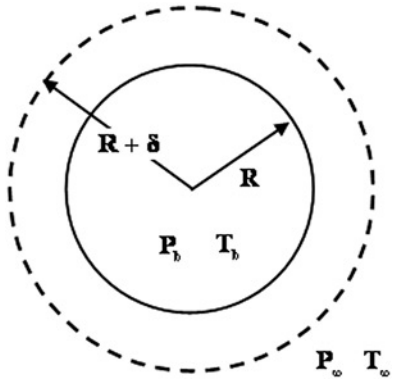

Figure 1.
Physical model for spherical bubble in liquid medium

The Gilmore equation describes the behaviour of a spherical bubble within a static, compressible and inviscid liquid subjected to a sinusoidal wave. As no gravity or other asymmetrical perturbating effects are considered, the equation describing the evolution of bubble radius as a function of time is (Gilmore, 1956):

$$R\ddot{R}\left(1-\frac{R}{C}\right)+\frac{3}{2}\dot{R}^2\left(1-\frac{R}{3C}\right)=H\left(1+\frac{\dot{R}}{C}\right)+\frac{R\dot{H}}{C}\left(1-\frac{\dot{R}}{C}\right), \tag{1}$$

where C and H are, respectively, the speed of sound and the liquid enthalpy at the interface between the gas-filled bubble and the liquid. The dots in Equation (1) refer to first- and second-order time derivation. To solve this ordinary differential equation, expressions for the enthalpy h and the speed of sound c in the bulk liquid are required as well. As the liquid is isentropic, h and c can be expressed as function of pressure p and density ρ in the liquid as follows:

$$h=\int_{P_\infty}^{p}\frac{dp}{\rho};\quad c=\sqrt{\frac{dp}{d\rho}}. \tag{2}$$

In deriving the above equations, it was assumed that the density of the liquid was a function of pressure only. Tait's equation is appropriate to describe the state of the liquid under these assumptions. The equation of state is given by:

$$\frac{p+B}{P_\circ+B}=\left(\frac{\rho}{\rho_\circ}\right)^A, \tag{3}$$

where the subscript 0 defines the ambient condition. $\rho_\circ = 1{,}800\,\mathrm{kg/m^3}$ is liquid density. The constant coefficients B and A are considered 3,500 and 6.25 bar, respectively, based on experimental NIST data for water pressure and density. The local enthalpy, h, and sound velocity, c, in the liquid at the instant liquid pressure p can be obtained by using the above equation of state in Equation (2) that is given by:

$$h=\frac{1}{\rho_\circ}\left(\frac{A}{A-1}\right)\left(\frac{1}{P_\circ+B}\right)^{-\frac{1}{A}}\left[(p+B)^{\frac{A-1}{A}}-(P_\infty-B)^{\frac{A-1}{A}}\right]. \tag{4}$$

$$c^2 = \frac{A}{\rho_\circ}(P_\circ - B)^{\frac{1}{A}}(p + B)^{\frac{A-1}{A}}. \tag{5}$$

The enthalpy and the speed of sound in the liquid at the interface can be obtained by using the pressure at the interface, P, in Equations (4) and (5) as follows:

$$H = \frac{1}{\rho_\circ}\left(\frac{A}{A-1}\right)\left(\frac{1}{P_\circ + B}\right)^{-\frac{1}{A}}\left[(P+B)^{\frac{A-1}{A}} - (P_\infty - B)^{\frac{A-1}{A}}\right], \tag{6}$$

$$C^2 = \frac{A}{\rho_\circ}(P_\circ - B)^{\frac{1}{A}}(P + B)^{\frac{A-1}{A}}. \tag{7}$$

The pressure at the interface in the liquid expresses as (Brennen, 1995):

$$P = P_b - \frac{2\sigma}{R} + 4\mu\frac{\dot{R}}{R}, \tag{8}$$

where $\mu = 0.025\,\mathrm{Ns/m^2}$ and $\sigma = 0.055\,\mathrm{N/m}$ are the surface tension and the dynamic viscosity of the liquid respectively.

The rapidly collapsing bubble may emit shock waves from the bubble wall in the outward direction. The dynamics of the pressure and velocity field in the liquid is calculated by using the Kirkwood and Bethe (1942) hypothesis. According to this assumption, the quantity Y, defined as $Y = r(h + (u^2/2)) = R(H + (1/2)\dot{R}^2)$ with r being the radial distance to the bubble centre and u being the velocity in the liquid, propagates in liquid with the velocity $c + u$:

$$\frac{\partial Y}{\partial t} = -(c+u)\frac{\partial Y}{\partial r}. \tag{9}$$

This homogeneous equation is then solved by the method of characteristics. The basis of this method is to calculate the velocity and the pressure field inside the liquid by integration of their time derivatives along characteristic curves, starting from their values at the bubble wall as obtained from the Gilmore model. The characteristic curved for Equation (9) are defined as curved $r(t)$ with a direction given by:

$$\frac{dr}{dt} = c(r(t)) + u(r(t)), \tag{10}$$

where $c(r(t))$ and $u(r(t))$ are the speed of sound and the velocity in the liquid along the characteristic curves. As these quantities vary along the characteristic curves, the following expressions for their time derivatives along the characteristic curves are used (Minsier and Proost, 2007):

$$\frac{du}{dt} = \frac{1}{r(c-u)}\left[(c+u)\frac{Y}{r}2uc^2\right]. \tag{11}$$

$$\frac{dp}{dt} = \frac{\rho_\circ}{r(c-u)} \left(\frac{p+B}{P_\circ + B}\right)^{\frac{1}{A}} \left[2c^2u^2 - \frac{c(c+u)}{r} Y\right]. \tag{12}$$

It is to be noted that the variables $c(r(t)), u(r(t))$, and $p(r(t))$ are written as u, c, and p in Equations (11) and (12).

3. Thermodynamic bubble motion

3.1 Analytical solutions for the gas inside a bubble

The mass conservation for the gas inside the bubble with spherical symmetry is given as:

$$\frac{\partial \rho_g}{\partial t} + \frac{1}{r^2}\frac{\partial}{\partial r}(\rho_g u_g r^2) = 0. \tag{13}$$

With decomposition of the density into centre and radial dependent parts such as:

$$\rho_g = \rho_{g\circ} + \rho_{gr}. \tag{14}$$

The continuity equation becomes:

$$\left[\frac{\partial \rho_{g\circ}}{\partial t} + \rho_{g\circ}\frac{1}{r^2}\frac{\partial}{\partial r}(u_g r^2)\right] + \left[\frac{\partial \rho_{gr}}{\partial t} + \frac{1}{r^2}\frac{\partial}{\partial r}(\rho_{gr} u_g r^2)\right] = 0. \tag{15}$$

The radial velocity profile inside the bubble may be written as Equation (20):

$$u_g = \frac{3\dot{R}}{R} r, \tag{16}$$

with the velocity profile, a set of solutions for the mass conservation equation may be obtained. These are:

$$\rho_{g\circ} R^3 = const, \tag{17}$$

and

$$\rho_{gr} = \frac{ar^2}{R^5}. \tag{18}$$

The constant a is related to the gas mass inside a bubble, m, by $(a/m) = (5/4\pi)[1 - (P_{b\circ}R_b^3/T_{b\circ})/(P'_\circ R_\circ^3/T_\infty)]$, where $P'_\circ = P_\circ + 2\sigma/R_\circ$. $P_{b\circ}$ and $T_{b\circ}$ are pressure and temperature at bubble centre respectively.

The momentum equations for the gas inside the bubble with spherical symmetry are given as:

$$\frac{\partial}{\partial t}(\rho_g u_g) + \frac{1}{r^2}\frac{\partial}{\partial r}(\rho_g u_g^2 r^2) + \frac{\partial P_b}{\partial r} = 0. \tag{19}$$

The gas pressure inside the bubble P_b can be obtained from the momentum equation with the density and velocity profile given in Equations (14) and (16), respectively.

$$P_b = P_{b\circ} - \frac{1}{2}\left(\rho_{g\circ} + \frac{1}{2}\rho_{gr}\right)\frac{\ddot{R}}{R}r^2 \tag{20}$$

Assuming that the internal energy for the gas inside a bubble is a function of gas temperature only as $de = C_v dT_b$, the energy equation for the gas inside the bubble may be written as:

$$\rho_g C_v \frac{DT_b}{Dt} = -\frac{P_b}{r^2}\frac{d}{dr}(r^2 u_g) - \frac{1}{r^2}\frac{d}{dr}(r^2 q_r). \tag{21}$$

Using the definition of enthalpy, the internal energy equation for the gas can also be written as:

$$\rho_g C_P \frac{DT_b}{Dt} = +\frac{DP_b}{Dt} - \frac{1}{r^2}\frac{d}{dr}(r^2 q_r). \tag{22}$$

Eliminating $D/Dt(= \partial/\partial t + u_g \partial/\partial r)T_b$ from Equations (21) and (22), one can obtain the following heat flow rate equation for the gas pressure inside bubble:

$$\frac{DP_b}{Dt} = -\frac{\gamma P_b}{r^2}\frac{\partial}{\partial r}(r^2 u_g) - \frac{\gamma - 1}{r^2}\frac{\partial}{\partial r}(r^2 q_r), \quad \gamma = \frac{C_p}{C_v}, \tag{23}$$

by substitution of Equations (14), (16), and (20) in the Equation (23), it becomes:

$$\frac{\gamma - 1}{r^2}\frac{\partial}{\partial r}(r^2 q_r) = -\left[\frac{dP_{b\circ}}{dt} + 3\gamma P_{b\circ}\frac{\dot{R}}{R}\right] + \frac{1}{2}\left(\rho_{g\circ} + \frac{1}{2}\rho_{gr}\right)\left[(3\gamma - 1)\frac{\dot{R}\ddot{R}}{R^2} + \frac{\dddot{R}}{R}\right]r^2. \tag{24}$$

The temperature distribution due to the non-uniformity of the pressure distribution which induced from abrupt increase and subsequent decrease in the bubble wall acceleration near the collapse point was neglected in this study. In fact, the term in Equation (20), which produced non-uniform pressure field is significant when the bubble wall acceleration exceeds 10^{12} m/s^2 (Kim *et al.*, 2007). With the uniform pressure approximation, Equation (24) can be written as:

$$\frac{(\gamma - 1)}{r^2}\frac{d}{dr}(r^2 q_\circ) = -\left[\frac{dP_{b\circ}}{dt} + 3kP_{b\circ}\frac{\dot{R}}{R}\right]. \tag{25}$$

A temperature profile of the gas inside the bubble can be obtained by using the Fourier law and Equation (25). That is (Kim *et al.*, 2007):

$$T_b(r) = \frac{B^*}{A^*}\left[-1 + \sqrt{\left(1 + \frac{A^*}{B^*}T_{b\circ}\right)^2 - 2\eta\frac{A^*}{B^*}(T_{bl} - T_\infty)\left(\frac{r}{R}\right)^2}\right], \tag{26}$$

where A^* and B^* are the coefficients in the temperature – dependent gas conductivity having a form such as $k_g = A^* T + B^*$ and $\eta = (R/\delta)(k_l/B^*)$, where $k_l = 0.4$ W/mK is

liquid conductivity. For Argon $A^* = 2.685 \times 10^{-5}$ J/msK^2 and $B^* = 1.347 \times 10^{-3}$ J/msK, for Xenon $A^* = 1.031 \times 10^{-5}$ J/msK^2 and $B^* = 3.916 \times 10^{-3}$ J/msK and for air $A^* = 5.528 \times 10^{-5}$ J/msK^2 and $B^* = 1.165 \times 10^{-2}$ J/msK.

The temperature at the bubble wall can easily be obtained from the Equation (26):

$$T_{bl} = \frac{B^*}{A^*}\left[-1 + \sqrt{\left(1 + \frac{A^*}{B^*}T_{b\circ}\right)^2 - 2\eta\frac{A^*}{B^*}(T_{bl} - T_\infty)}\right]. \tag{27}$$

At the bubble centre, the state equation for an ideal gas is $P_{b\circ}R^3/T_{b\circ} = const.$ Therefore:

$$\frac{dT_{b\circ}}{dt} = \frac{T_{b\circ}}{P_{b\circ}}\frac{dP_{b\circ}}{dt} + \frac{3T_{b\circ}\dot{R}}{R}. \tag{28}$$

The above equation can be written, with the help of Equation (25) as follows:

$$\frac{dT_{b\circ}}{dt} = -3(\gamma - 1)\frac{T_{b\circ}\dot{R}}{R} - (\gamma - 1)\frac{T_{b\circ}}{P_{b\circ}}\frac{1}{r^2}\frac{d}{dr}(r^2 q_\circ). \tag{29}$$

The bubble centre temperature can be obtained by using the Fourier law and Equation (28). That is:

$$\frac{dT_{b\circ}}{dt} = \frac{3(\gamma - 1)T_{b\circ}}{R}\frac{dR}{dt} - \frac{6(\gamma - 1)k_l(T_{b\circ} - T_\infty)}{\delta R P_{b\circ}}. \tag{30}$$

The temperature distribution in the liquid layer adjacent to the bubble wall, which is important to determine the heat transfer through the bubble wall, is assumed to be quadratic (Theofanous, 1969), such as:

$$\frac{T - T_\infty}{T_{bl} - T_\infty} = (1 - \xi)^2, \quad \xi = (r - R)/\delta. \tag{31}$$

Such second-order curve satisfies the following boundary conditions:

$$T(R, t) = T_{bl}, \quad T(R + \delta, t) = T_\infty, \quad \left(\frac{\partial T}{\partial r}\right)_{\mathrm{r=R+\delta}} = 0. \tag{32}$$

The energy conservation equation for liquid under the influence of bubble wall motion is expressed by:

$$\frac{\partial T}{\partial t} + u_r\frac{\partial T}{\partial r} = \frac{\alpha_l}{r^2}\frac{\partial}{\partial r}\left(r^2\frac{\partial T}{\partial r}\right), \tag{33}$$

where $\alpha_l = k_l/\rho_\circ C_P$ is the thermal diffusivity, and the radial velocity of liquid due to bubble motion can be obtained from mass conservation for an incompressible liquid $\nabla.\mathrm{u_r} = 0$. That is:

$$u_r = \left(\frac{R}{r}\right)\dot{R}. \tag{34}$$

Integrating Equation (33) from $r = R$ to $r = R + \delta$ yields:

$$\int_R^{R+\delta} r^2 \frac{\partial T}{\partial t} dr + \int_R^{R+\delta} u_r r^2 \frac{\partial T}{\partial r} dr = \int_R^{R+\delta} \alpha_l \frac{\partial}{\partial r}\left(r^2 \frac{\partial T}{\partial r}\right) dr, \tag{35}$$

with the temperature profile and boundary conditions given in Equations (31) and (32), and the velocity profile in the liquid (Equation (34)), the above equation become (Ryu and Kwak, 1992):

$$\begin{aligned}\left[1 + \frac{\delta}{R_b} + \frac{3}{10}\left(\frac{\delta}{R_b}\right)^2\right]\frac{d\delta}{dt} = \frac{6\alpha}{\delta} - \left[2\frac{\delta}{R_b} + \frac{1}{2}\left(\frac{\delta}{R_b}\right)^2\right]\frac{dR_b}{dt} \\ - \delta\left[1 + \frac{1}{2}\frac{\delta}{R_b} + \frac{1}{10}\left(\frac{\delta}{R_b}\right)^2\right]\frac{1}{T_{bl} - T_\infty}\frac{dT_{bl}}{dt}.\end{aligned} \tag{36}$$

3.2 Polytropic approximation

In the previous research, usually the gas inside the bubble is assumed uniform. In all gas state equations, the pressure is described as a function of density and the temperature. The density can be calculated from the bubble volume and the initial gas content of the bubble, as no mass exchange is considered between the bubble and the liquid. However, temperature is unknown. This is done by assuming that the gas is polytropic. A Vander Waals equation with polytropic exponent of γ was employed to obtain the gas pressure inside a uniformly compressed bubble:

$$P_b = \left(P_\circ + \frac{2\sigma}{R}\right)\left(\frac{R_\circ^3 - h^3}{R^3 - h^3}\right)^\gamma, \tag{37}$$

where $h = R_\circ/8.5$ is the hard-core Vander Waals radius and γ is the polytropic index. For calculating the temperature, the following relation with variable polytropic indexes of γ, which is related to the thermal diffusivity of gas and liquid and driving sound frequency (Prosperetti, 1977), may be employed:

$$\frac{T_b}{T_\infty} = \left(\frac{R_\circ^3 - h^3}{R^3 - h^3}\right)^{\gamma - 1}. \tag{38}$$

For a bubble under ultrasound frequency of kHz range the polytropic index needed to calculated pressure and temperature is about 1.3 (Kim *et al.*, 2007).

4. Results and discussion

The initial conditions of $R = R_\circ, \dot{R} = 0, P_b = P_\circ, T_{bl} = T_\infty, T_{b\circ} = T_\infty$, and $\delta = 5.0R_\circ$, Equations (1), (6)-(8), (27), (30), and (36) are simultaneously solved by using the fourth order Runge-Kutta numerical method to obtain the next time step values of $\dot{R}_b, R_b, T_{b\circ}, T_{bl}$, and δ. By calculated bubble centre density, $\rho_{g\circ}$, from Equation (17),

the gas pressure at the bubble centre can be obtained from the ideal gas law $P_{b\circ}/\rho_{g\circ}T_{b\circ} = \text{const}$. This calculated was repeated up to the desired time step. In this calculation, we let $d\delta/dt = 0$ to avoid an infinite value of boundary layer thickness, provided that the absolute value of $|T_{bl} - T_{\infty}| < 0.5\,^{\circ}\text{C}$.

The bubble radius and ambient (driving) pressure vs time is illustrated in Figure 2. The bubble radius is calculated by this presented scheme and also by polytropic assumption. The ambient pressure is $P_{\infty} = P_{\circ} + P_e \sin(2\pi ft)$, and P_e and f are the driving pressure amplitude and frequency. The ultrasound frequency of 28.5 kHz and amplitude of 1.42 bars in an aqueous solution of sulphuric acid is applied. The results are compared with the experimental data obtained originally by Flannigan *et al.* (2006). The initial (equilibrium) radius of this Argon bubble is $R_{\circ} = 13\,\mu\text{m}$. The bubble radius increases by decreasing pressure. A time, lag between the occurrence of minimum pressure and maximum bubble radius is observed. But, the bubble collapses before reaching maximum pressure. The polytropic assumption suffers to predict maximum radius. This assumption yields quantitatively incorrect results because the thermal damping due to the finite heat transfer across the bubble wall cannot be taken into account. The present numerical calculation well matches with the experimental data for predicting maximum radius. Close agreement between the calculated result and experimental can be seen.

The time-dependent thermal boundary layer thickness calculated from Equation (36) around the collapse point is shown in Figure 3. The minimum value of boundary layer thickness is $\delta_{\min} = 1.5\,\mu\text{m}$ that occurs in collapse point. Figure 4 shows the calculated time-dependent temperatures at the bubble centre. The calculated gas temperature at the

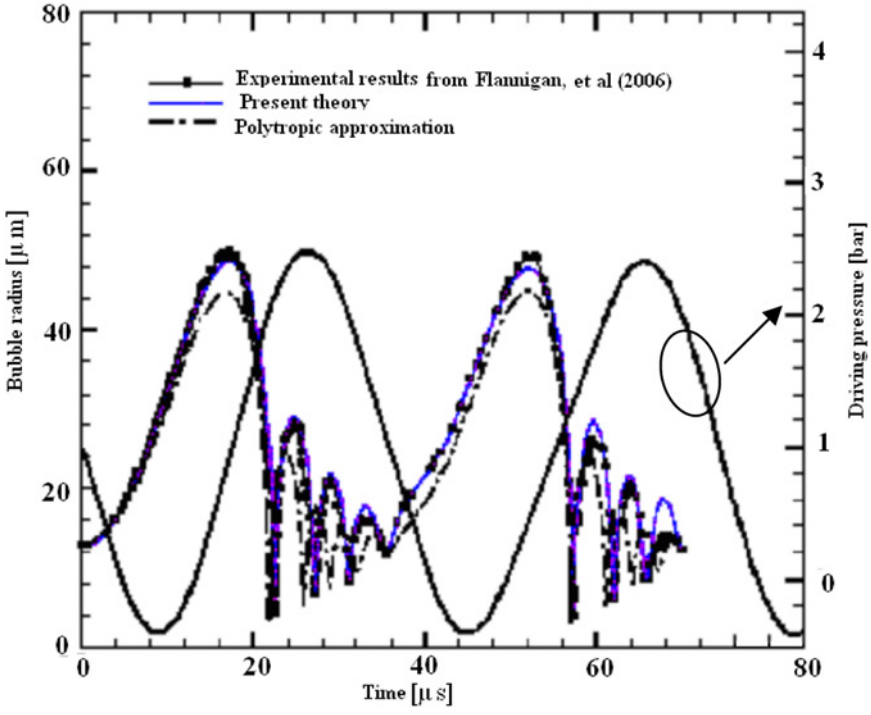

Figure 2.
Theoretical and experimental radius-time curve for an argon bubble of $R_{\circ} = 13\,\mu\text{m}$ at $P_a = 1.42\,\text{bar}$ and $f = 28.5\,\text{kHz}$

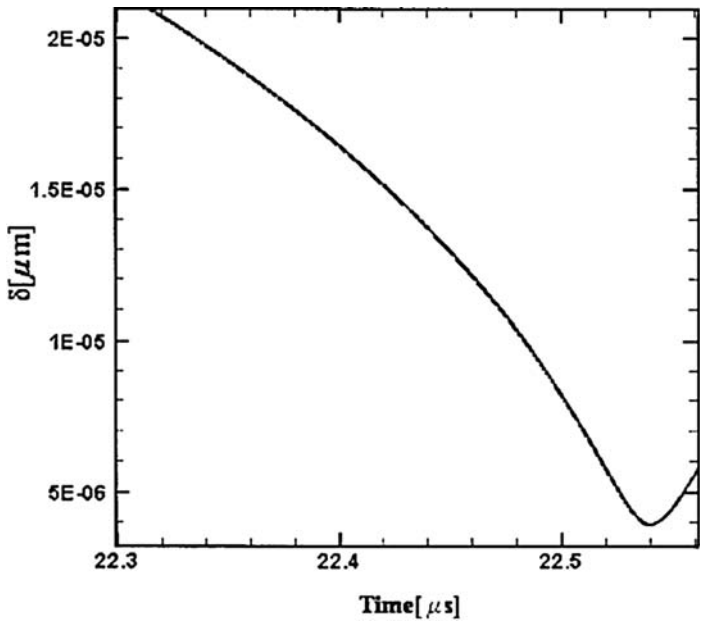

Figure 3.
Boundary layer thickness vs time during the collapse of bubble

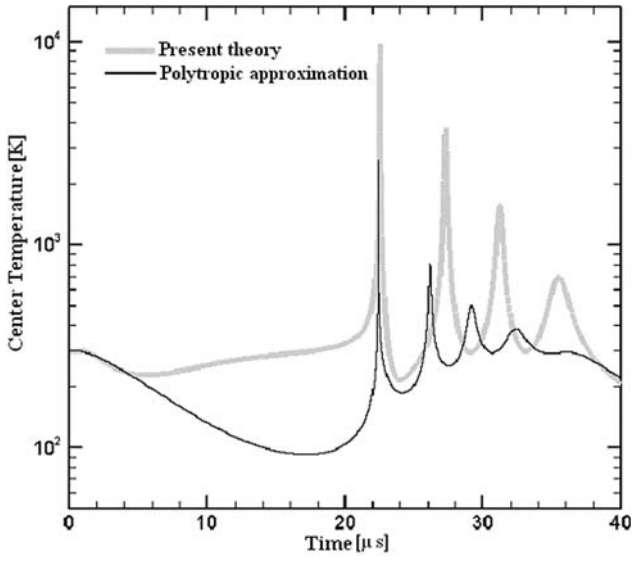

Figure 4.
Calculated bubble centre temperature for the bubble shown in Figure 2

maximum size of the bubble is about 290 K, which is the same as the one at equilibrium condition. On the other hand, considerably lower temperature as low as 100 K is achieved at the point of the maximum bubble radius when the bubble evolution was assumed to be proceeded by the polytropic process with $n = 1.3$. The calculated peak temperature at the collapse point is about 9,300 K, which is close to the observed value of 10,000 K

(Flannigan *et al.*, 2006). However, the polytropic approximation considerably underestimates the gas temperature of 2,600 K at the collapse point.

The gas pressure at the bubble centre vs time is shown in Figure 5. The pressure changes suddenly when the bubble collapses. Such an abrupt increase and subsequent decrease in the bubble wall pressure may produce an outgoing shock wave. The calculated pressure at the collapse point is about 1,005 atm, which close to the observed value of 1,090 atm (Flannigan *et al.*, 2006). However, a considerable overestimation in the gas pressure at the collapse point with the polytropic assumption is seen.

Figure 6 shows the time-dependent bubble wall velocity. Figure 6(a) shows this velocity for present theory and Figure 6(b) shows it by polytropic assumption. The

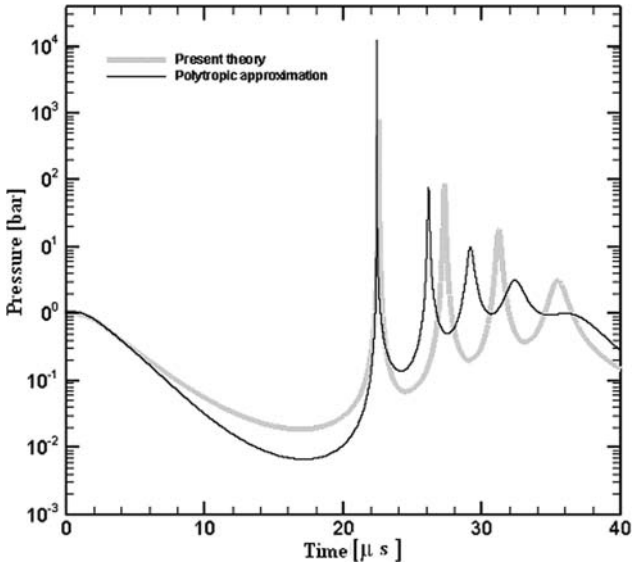

Figure 5.
Calculated bubble centre pressure for the bubble shown in Figure 2

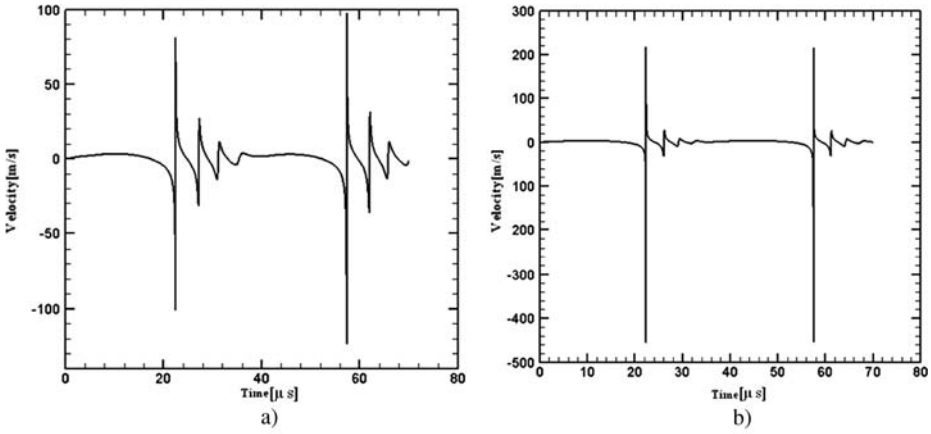

Notes: (a) Present theory and (b) polytropic approximation

Figure 6.
Calculated liquid velocity at shock front for the bubble shown in Figure 2

calculated magnitude of the minimum velocity at the collapse point is about 110 m/s Figure 6(a), which is close to the observed value of 100 m/s. However, the magnitude of the minimum velocity obtained by using polytropic relationship is about 460 m/s Figure 6(b), which is much higher than the observed value.

Figure 7 depicts the calculated strength Figure 7(a) and liquid velocity Figure 7(b) of the shock waves emitted upon bubble collapse at distance $r = 100$ and 300 μm from bubble centre. The shock wave takes about 22.6 μs to arrive at 0.1 mm from the bubble centre and the magnitude of the shock wave strength at this point is about 37 atm, while the value related to the polytropic approximation is about 92 atm which arrive this point at 22.47 μs. This means that the polytropic approximation overestimates the magnitude of the shock wave strength at specific point from the bubble centre. Also, Figure 7(b) shows the liquid velocity at the shock front. The polytropic approximation overestimates the peak strength and the wave velocity.

The time histories of bubble radius obtained by present theory for gases with different heat conductivity are shown in Figure 8. In all cases the initial radius ($R_\circ$) is 13 μm, the driving pressure frequency and amplitude are 28.5 kHz and 1.42 bars, respectively. The result for three different heat conductivity of gases ($K_{Air} \gg K_{Argon} > K_{Xenon}$) is compared. The trend of $R(t)$ for all gases is similar. Air bubble has the most discrepancy with the other fluids. At the first loop of oscillation, the maximum bubble radius for air is larger than the others. While the second, the third, and the forth loop are almost the same and the maximum bubble radius for xenon is larger than the argon and air respectively.

The bubble radius around the first collapse is shown in Figure 9. Xenon bubble collapse occurs earlier than the argon and air bubble. Minimum bubble radius for the air is the smallest. Because of higher thermal conductivity of air, less temperature gradient inside the bubble occurs for the air bubble as shown in Figure 10. The gas temperature at the bubble wall and the average temperature becomes higher, so that the pressure inside the bubble has a higher value correspondingly for the air bubble.

The strength of the shock wave for the mentioned gases is illustrated in Figure 11. The shock wave strength for air bubble is the highest.

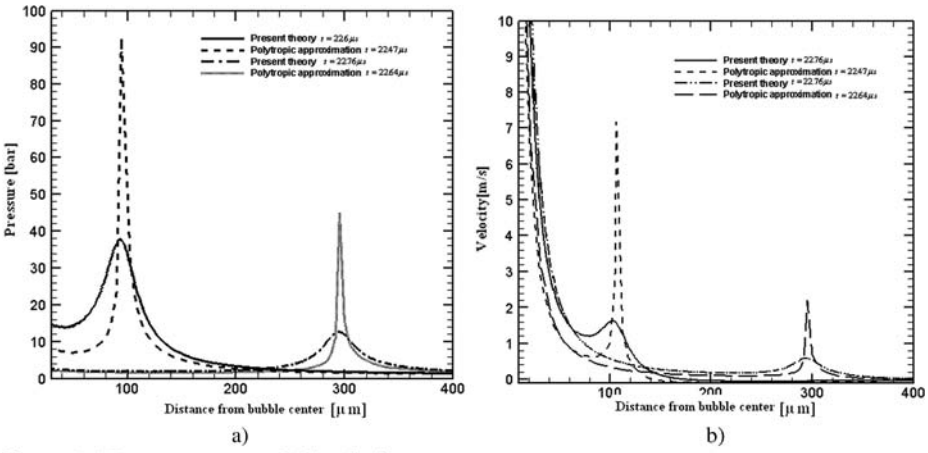

Figure 7.
The intensity of travelling wave at a specific time emitted upon bubble collapse at distance $r = 100$ and 300 μm from bubble centre for the bubble shown in Figure 2

Notes: (a) Pressure wave and (b) velocity wave

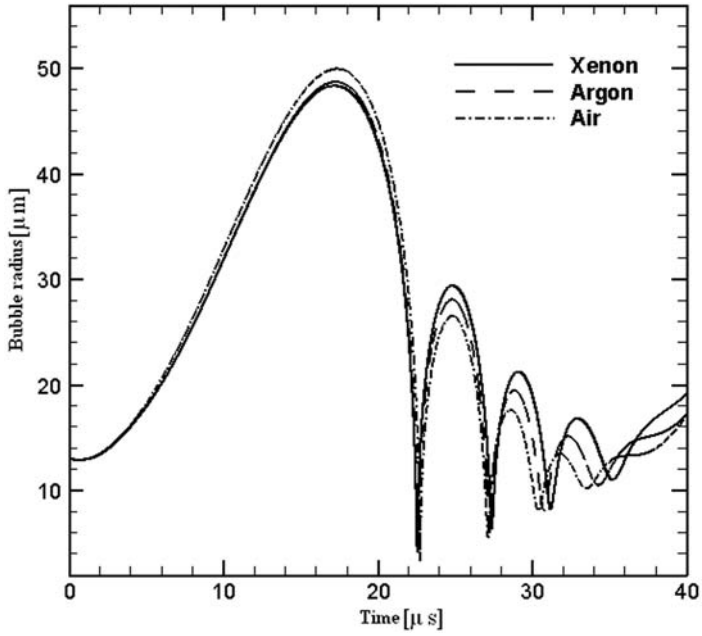

Figure 8.
Theoretical radius-time curves for bubbles with different heat conductivities and initial radius of $R_\circ = 13\,\mu m$ at $P_a = 1.42\,bar$ and $f = 28.5\,kHz$

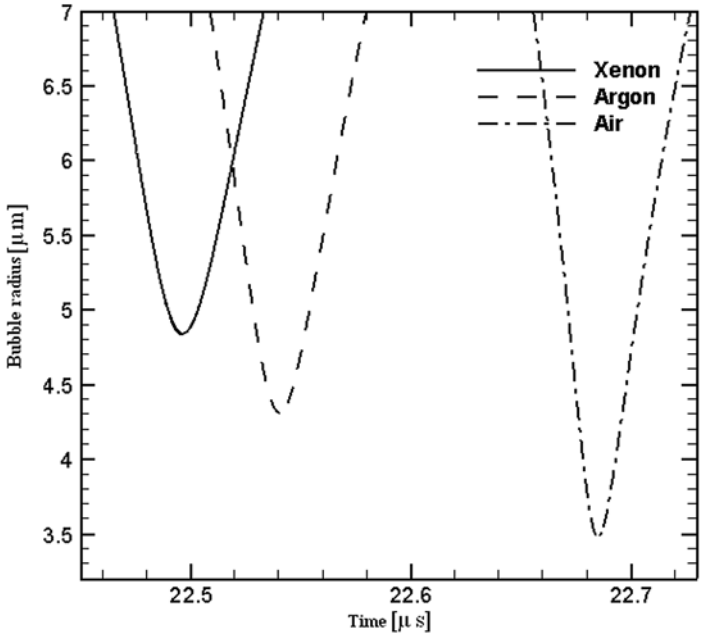

Figure 9.
The calculated radius-time curves near the collapse point for the bubble shown in Figure 8

Figure 12 shows the bubble radius-time curves for an Argon bubble of $R_\circ = 10\,\mu m$ driven with an ultrasound frequency of 28.5 kHz and different amplitudes. The maximum bubble radius increases by increasing the amplitude at the first loop. In the second, third, and forth loop, the maximum bubble radius size is not affected by the amplitude.

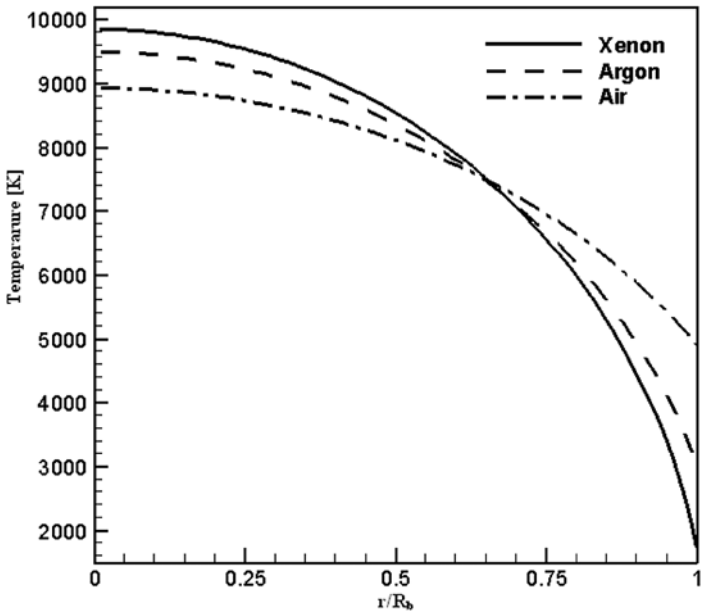

Figure 10.
The temperature distributions at the collapse point for the bubble shown in Figure 8

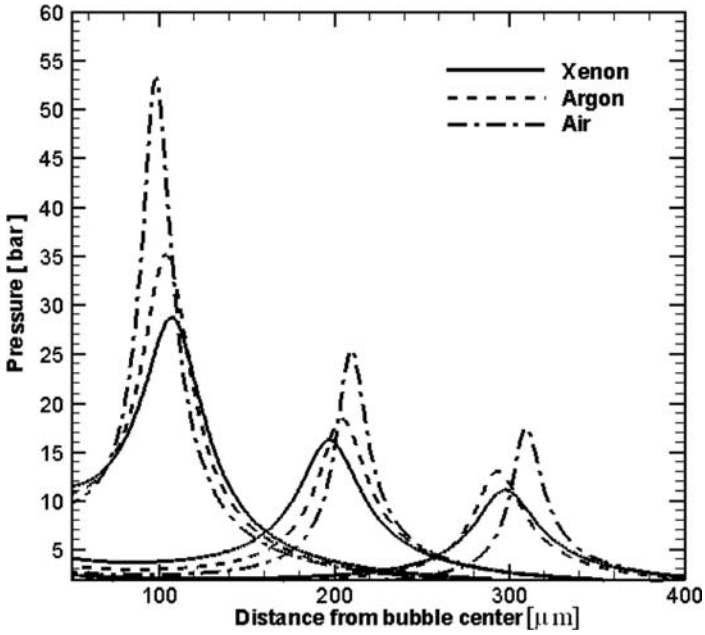

Figure 11.
The strengths of shock wave for the bubble shown in Figure 8

The bubble centre temperature for Argon bubble is shown in Figure 13 as a function of the initial bubble radius ($R_\circ$) and ultrasound pressure amplitude (P_a). It is seen that the bubble centre temperature increases with the acoustic amplitude, and decreases as a function of $R_\circ$. Figures 14 and 15 show that this behaviour is

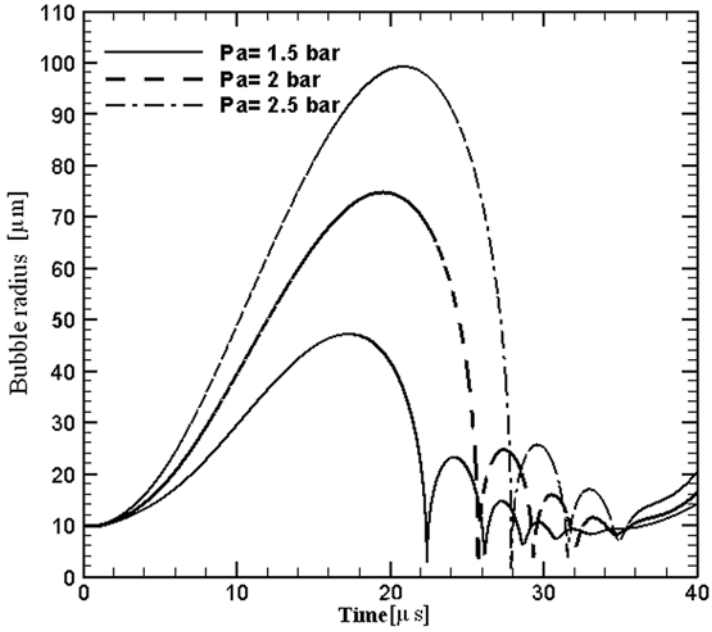

Figure 12.
Theoretical radius-time curves of different amplitude driven pressure for Argon bubble of $R_\circ = 10\,\mu\text{m}$ and $f = 28.5\,\text{kHz}$

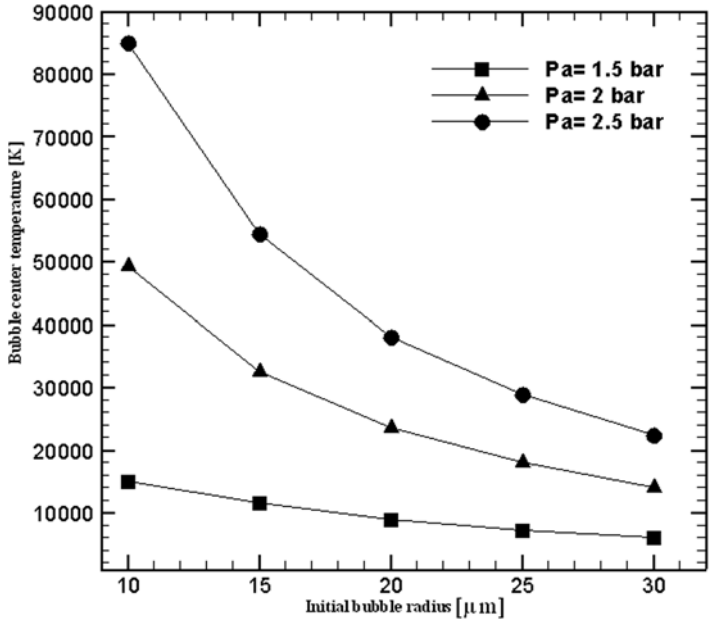

Figure 13.
Bubble centre temperature at collapse point for Argon bubble

qualitatively similar to the bubble centre pressure and maximum velocity at the bubble wall respectively.

The strength of shock wave emitted upon bubble collapse for an initial bubble radius $R_\circ = 13\,\mu\text{m}$ and two acoustic amplitudes $P_a = 1.5$ and $P_a = 2\,\text{bar}$ is shown in Figure 16.

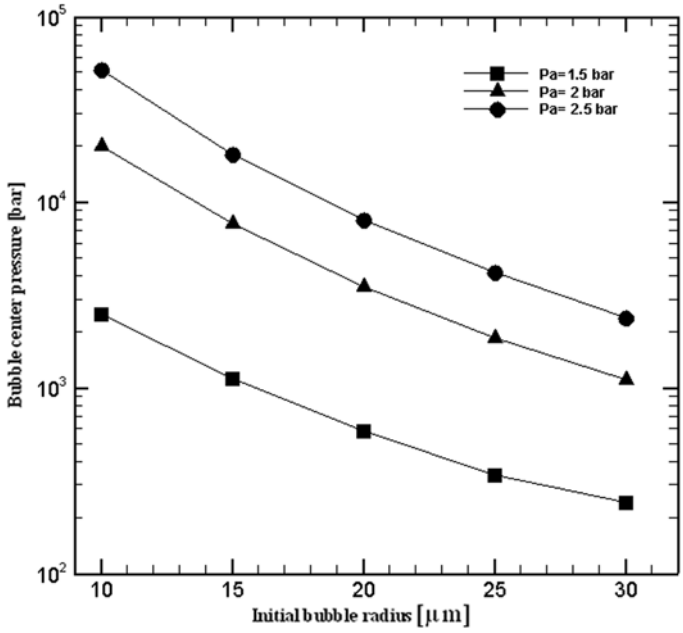

Figure 14.
Bubble centre pressure at collapse point for Argon bubble

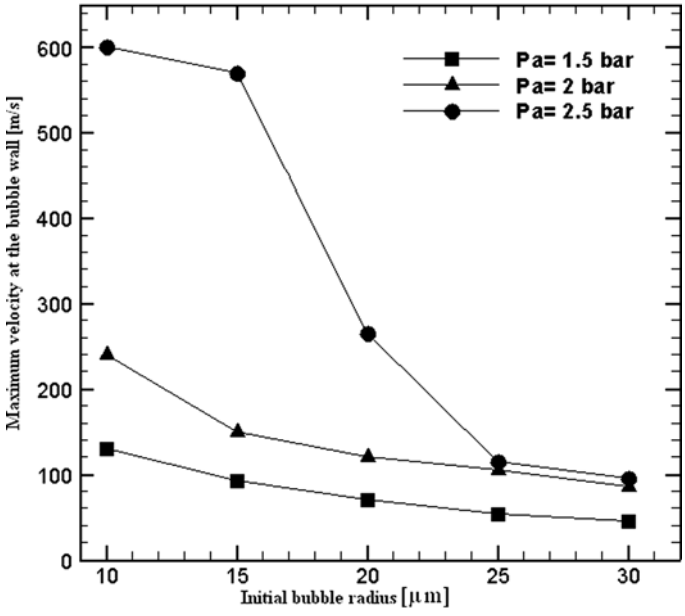

Figure 15.
Maximum velocity at the bubble wall for Argon bubble

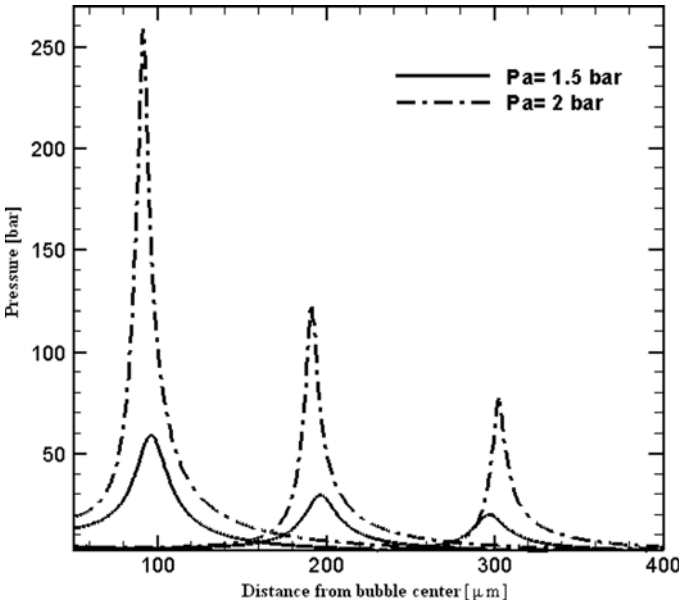

Figure 16.
The strengths of shock wave for the Argon bubble of different driven pressure, $R_\circ = 13\,\mu$m and $f = 28.5$ kHz

It is seen that for each pressure amplitude, the magnitude of the shock wave decreases as 1/r and increases by pressure amplitude. As shown Figure 17 the magnitude of the shock wave for bubble with small initial radius is higher than bubble with high initial radius.

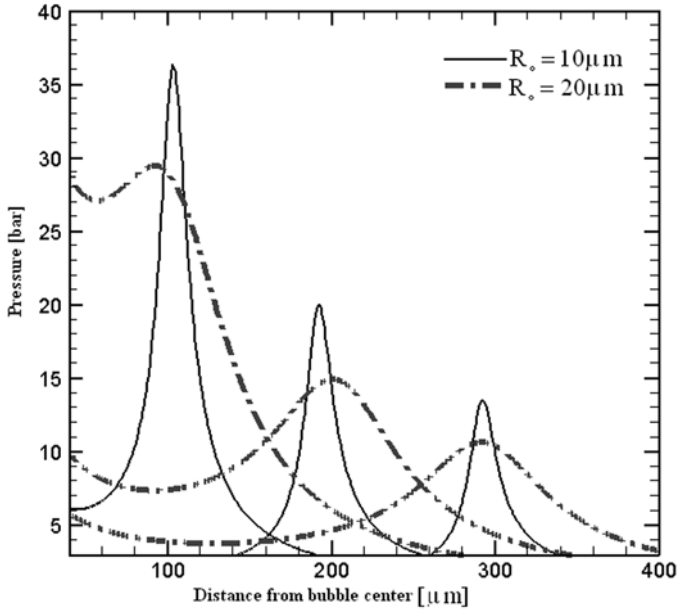

Figure 17.
The strengths of shock wave for the Argon bubble of different initial radius, $P_a = 1.42$ bar and $f = 28.5$ kHz

5. Conclusions

A mathematical model for a spherically symmetric gas bubble under ultrasound in aqueous sulphuric acid solution is presented. This model accounts for gas and liquid compressibility, gas heat transfer inside the bubble and liquid layer adjacent to the bubble wall. A number of numerical simulations of bubble dynamics have been done on the basis of this model and the following conclusions have been reached:

- Heat transfer inside the bubble as well as in the liquid layer adjacent to the bubble wall is a very important factor, which affects the bubble motion and the magnitude of shock wave.
- Polytropic approximation overestimates the peak pressure and underestimates the peak temperature for an ultrasonic gas bubble.
- Polytropic approximation causes overestimation the strength and velocity of shock wave.
- Less temperature gradient inside the bubble occurs for the gas with higher thermal conductivity. However, the average temperature so that the pressure inside the bubble and shock wave strength becomes higher.
- The maximum bubble radius increases with the amplitude of the acoustic field.
- The bubble centre temperature, pressure and maximum bubble wall velocity increases with amplitude of the acoustic filed and decreases with initial bubble radius.
- The strength of shock wave emitted upon bubble collapse increases with the amplitude of driven pressure and decreases with the initial bubble radius.

References

Brennen, C.E. (1995), *Cavitation and Bubble Dynamics*, Oxford University Press, Oxford.

Flannigan, D.J., Hopkins, S.D. and Camara, C.G. (2006), "Measurement of pressure and density inside a single sonoluminescing bubble", *Physical Letters*, Vol. 96, p. 204301.

Fujikawa, S. and Akamatsu, T. (1980), "Effects of the non-equilibrium condensation of vapour on the pressure wave produced by the collapse of a bubble in a liquid", *Journal of Fluid Mechanics*, Vol. 97, pp. 481-512.

Gilmore, F.R. (1956), *Hydrodynamics Laboratory Report 26.4*, California Institute of Technology, Pasadena, CA.

Herring, C. (1941), "Theory of the pulsations of the gas bubble produced by an underwater explosion", OSRD Report No. 236, The Library of Congress, Washington, DC.

Hickling, R. and Plesset, M.S. (1964), "Collapse and rebound of a spherical bubble in water", *Physics of Fluids*, Vol. 7, pp. 7-14.

Hilgenfeldt, S., Brenner, M.P., Grossmann, S. and Lohse, D. (1998), "Analysis of Rayleigh-Plesset dynamics for sonoluminescing bubbles", *Journal of Fluid Mechanics*, Vol. 365, pp. 171-204.

Ivany, R.D. and Hammitt, F.G. (1965), "Cavitation bubble collapse in viscous, compressible liquids – numerical analysis", *ASME Journal of Basic Engineering*, Vol. 87, pp. 977-85.

Kamath, V.A., Prosperetti, A. and Egolfopoulos, F.N. (1993), "A theoretical study of sonoluminescence", *Journal of the Acoustical Society of America*, Vol. 94, pp. 248-60.

Kim, K.Y., Byun, K. and Kwak, H. (2007), "Temperature and pressure fields due to collapsing bubble under ultrasound", *Chemical Engineering Journal*, Vol. 132, pp. 125-35.

Kirkwood, J.G. and Bethe, H.A. (1942), "The pressure wave produced by an underwater explosion", OSRD Report No. 588, The Library of Congress, Washington, DC.

Kwak, H. and Na, J.H. (1996), "Hydrodynamic solutions for a sonoluminescing gas bubble", *Physical Review Letter*, Vol. 77, pp. 4454-7.

Minsier, V. and Proost, J. (2007), "Shock wave emission upon spherical bubble collapse during cavitation-induced megasonic surface cleaning", *Journal of Ultrasonic Sonochemistry*, Vol. 15 No. 4, pp. 598-604.

Moss, W.C., Clarke, D.B., White, G.W. and Young, D.A. (1994), "Hydrodynamic simulations of bubble collapse and picoseconds sonolumirrescence", *Physics of Fluid*, Vol. 6, pp. 2976-85.

Philipp, A. and Lauterborn, W. (1998), "Cavitation erosion by single laser-produced bubbles", *Journal of Fluid Mechanics*, Vol. 361, pp. 75-116.

Plesset, M.S. and Prosperetti, A. (1997), "Bubble dynamics and cavitation", *Annual Review of Fluid Mechanics*, Vol. 9, pp. 145-85.

Prosperetti, A. (1977), "Thermal effects and damping mechanism in the forced radial oscillations of gas bubbles in liquid", *Journal of Acoustical Society*, Vol. 61, pp. 17-27.

Prosperetti, A. and Hao, Y. (1999), "Modeling of spherical gas bubble oscillations and sonoluminescence", *Philosophical Transactions of the Royal Society of London Series A*, Vol. 357, pp. 203-23.

Ryu, J.C. and Kwak, Y.H. (1992), "Bifurcation phenomena for the pumped bubble oscillations in periodically driven pressure fields", In *Bifurcation Phenomena and Chaos in Thermal Convection*, ASME, New York, NY, Vol. HTD-214, pp. 1-8.

Schneider, A.J.R. (1949), "Some compressibility effects in cavitation bubble dynamics", PhD thesis, California Institute of Technology, Pasadena, CA.

Theofanous, T., Biasi, L. and Isbin, H.S. (1969), "A theoretical study on bubble growth in constant and time-dependent pressure fields", *Chemical Engineering Science*, Vol. 24, pp. 885-97.

Tomita, Y. and Shima, A. (1977), "On the behaviour of a spherical bubble and the impulse pressure in a viscous compressible liquid", *Bulletin of JSME*, Vol. 20, pp. 1453-60.

Weninger, R., Evanse, P.G. and Putterman, S.J. (2001), "Comment on Mie scattering from a sonoluminescing bubble with high spatial and temporal resolution", *Physical Review*, Vol. 61, pp. 5253-6.

Wu, C.C. and Robert, P.H. (1993), "Bubble shape instability and sonoluminescence", *Physical Review Letters*, Vol. 70, pp. 3424-7.

Further reading

Knapp, R.T., Daily, J.W. and Hammitt, F.G. (1970), *Cavitation*, McGraw-Hill, New York, NY.

Kwak, H. and Yang, H. (1995), "An aspect of sonluminescence from hydrodynamic theory", *Journal of the Physical Society of Japan*, Vol. 64, pp. 1980-92.

Corresponding author

Mehrzad Shams can be contacted at: shams@kntu.ac.ir